Article

Ground Level PM$_{2.5}$ Estimates over China Using Satellite-Based Geographically Weighted Regression (GWR) Models Are Improved by Including NO$_2$ and Enhanced Vegetation Index (EVI)

Tianhao Zhang [1], Wei Gong [1,2,*], Wei Wang [1,*], Yuxi Ji [1], Zhongmin Zhu [1,3] and Yusi Huang [1]

[1]   State Key Laboratory of Information Engineering in Surveying, Mapping, and Remote Sensing,
      Wuhan University, Wuhan 430079, China; tianhaozhang@whu.edu.cn (T.Z.); jiyuxi_ss@163.com (Y.J.);
      zhongmin.zhu@whu.edu.cn (Z.Z.); mavis_huang@whu.edu.cn (Y.H.)
[2]   Collaborative Innovation Center for Geospatial Technology, Wuhan 430079, China
[3]   College of Information Science and Engineering, Wuchang Shouyi University, Wuhan 430064, China
[*]   Correspondence: weigong@whu.edu.cn (W.G.); wangweicn@whu.edu.cn (W.W.);
      Tel.: +86-135-1724-1678 (W.G.); +86-135-4536-0741 (W.W.)

Abstract: Highly accurate data on the spatial distribution of ambient fine particulate matter (<2.5 μm: PM$_{2.5}$) is currently quite limited in China. By introducing NO$_2$ and Enhanced Vegetation Index (EVI) into the Geographically Weighted Regression (GWR) model, a newly developed GWR model combined with a fused Aerosol Optical Depth (AOD) product and meteorological parameters could explain approximately 87% of the variability in the corresponding PM$_{2.5}$ mass concentrations. There existed obvious increase in the estimation accuracy against the original GWR model without NO$_2$ and EVI, where cross-validation R^2 increased from 0.77 to 0.87. Both models tended to overestimate when measurement is low and underestimate when high, where the exact boundary value depended greatly on the dependent variable. There was still severe PM$_{2.5}$ pollution in many residential areas until 2015; however, policy-driven energy conservation and emission reduction not only reduced the severity of PM$_{2.5}$ pollution but also its spatial range, to a certain extent, from 2014 to 2015. The accuracy of satellite-derived PM$_{2.5}$ still has limitations for regions with insufficient ground monitoring stations and desert areas. Generally, the use of NO$_2$ and EVI in GWR models could more effectively estimate PM$_{2.5}$ at the national scale than previous GWR models. The results in this study could provide a reasonable reference for assessing health impacts, and could be used to examine the effectiveness of emission control strategies under implementation in China.

Keywords: nationwide ambient PM$_{2.5}$; MODIS (Moderate Resolution Imaging Spectroradiometer) AOD; satellite-derived NO$_2$ column density; enhanced vegetation index; geographically weighted regression

1. Introduction

Numerous previous studies reported that atmospheric particulate matter emitted from both anthropogenic and natural sources exert influences on climate change and environmental deterioration [1,2]. Many epidemiological studies have shown that exposure to fine suspended particles with aerodynamic diameter less than 2.5 μm (PM$_{2.5}$) are linked with cardiovascular and respiratory diseases [3–6]. With vast consumption of energy and rapid economic development, China has suffered from severe PM$_{2.5}$ pollution and the related social problems have caused wide concerns [7,8]. Although an air quality monitoring network has been established in China since 2013, large-scale estimation of

Int. J. Environ. Res. Public Health **2016**, *13*, 1215

2 of 12

PM$_{2.5}$ is not practical due to the limited spatial coverage of the monitoring stations [9]. Consequently, there exists an urgent need to acquire a spatially resolved characterization of human exposure to PM$_{2.5}$ at the national scale in China [10].

In order to make up for the blanks in ground measurements, methods using remote sensing by satellite have been adopted to estimate ground-level PM$_{2.5}$ mass concentrations [11,12]. There exists a direct relationship between the atmospheric particles and satellite-derived Aerosol Optical Depth (AOD) because AOD represents the quantity of light removed from a beam by the role of aerosol scattering or absorption during its path [13–16]. Previous studies proposed establishing empirical models to correlate ground-level PM$_{2.5}$ and satellite derived AOD (e.g., linear, nonlinear, and logarithmic models) [13,17–19]. Superior models have been established for better predicting the PM$_{2.5}$ concentrations combined with meteorological parameters or based on atmospheric transport models, such as the mixed effects model (MEM) [20], the artificial neural network model (ANN) [17,21,22], and the chemical transport model (CTM) [23]. Since the correlation between AOD and PM$_{2.5}$ should vary along with the spatial context due to different geographical areas possessing different aerosol types [9,24,25], the Geographically Weighted Regression (GWR) model, which better constrains the spatial variability in a large-region regression, has been adopted to estimate geographical elements in large regions [26,27]. The particulate matter vertical distribution has been additionally taken into consideration from a physics perspective, which could improve the correlation between PM$_{2.5}$ and AOD [28]. Moreover, previous study of the GWR model combined with physical corrections indicated that the atmospheric vertical feature could be embedded in the GWR model via Planetary Boundary Layer Height (PBLH) for better estimation accuracy of atmospheric particulates at the national scale [29]. Nevertheless, these statistical models rely greatly on observation from satellites and meteorological parameters, and anthropogenic emissions need additionally consideration, such as traffic density [30].

In this study, the molar concentration of OMI-NO$_2$ (Ozone Measuring Instrument) and MODIS-EVI (Moderate Resolution Imaging Spectroradiometer) were introduced into the GWR model, considering that these two variables can be measured via satellites at a large spatial scale. A different GWR model was then established to predict PM$_{2.5}$ concentrations at the national scale using fused MODIS-AOD based on a dark target and deep blue algorithm, meteorological parameters, daily tropospheric NO$_2$ molar concentration, and fixed 16-day composite EVI. For quantitatively evaluating the model performance, a leave-one-out cross-validation was adopted to demonstrate the relationship between measured PM$_{2.5}$ and estimated PM$_{2.5}$, and results from the previous GWR model without NO$_2$ and EVI were also provided for contrast. Moreover, the two-year annual spatial distribution of the satellite-derived PM$_{2.5}$ at the national scale was demonstrated, analyzed, and discussed.

2. Materials and Methods

2.1. Ground PM$_{2.5}$ Measurements

Hourly ground-level PM$_{2.5}$ measurements in China from 1 January 2014 to 31 December 2015 were collected primarily from the official website of the China Environmental Monitoring Center (CEMC) [31] As demonstrated in Figure 1, more than 1300 air quality monitoring stations have been built up covering residential cities in all provinces of China by the end of 2014. According to the officially released documents of the Chinese Ministry of Environmental Protection (MEP), the PM$_{2.5}$ data were measured using the tapered element oscilating microbalance method (TEOM) or the beta-attenuation method, combined with periodic calibration [32].
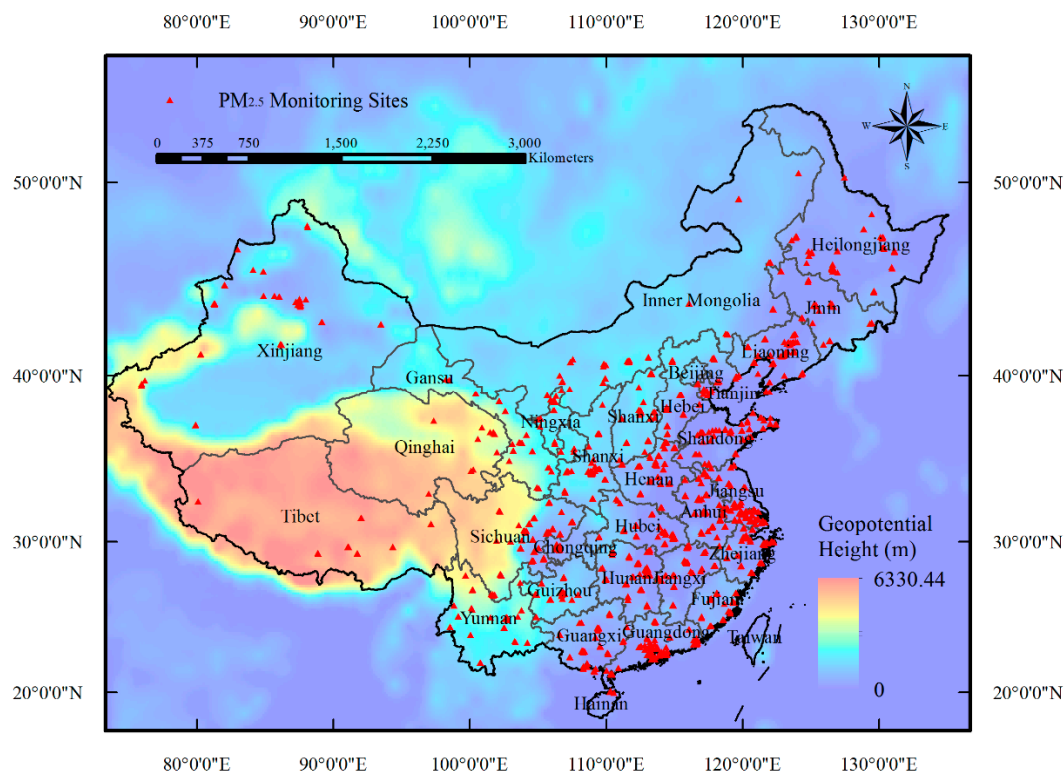
Figure 1. Spatial distribution of PM$_{2.5}$ monitoring stations (solid red dots) from which data were gathered in this study.

2.2. Moderate Resolution Imaging Spectroradiometer (MODIS) Aerosol Products

The MODIS aboard the NASA Earth Observing System (EOS) satellite, Aqua, was shown to provide aerosol products with assured quality when compared with other satellite sensors [33–36]. In this study, we use the Collection 6 (C6) aerosol products because these products have generally been proven to attain fine accuracy by validation against ground monitoring observations of sun photometers from the Aerosol Robotic Network (AERONET) in China [37,38]. The Aqua AOD datasets used in this study, which were retrieved based on the relationship between the radiation value of specific bands over land and the aerosol optical depth, were distributed in Hierarchical Data Format (HDF) format from the NASA Goddard Space Flight Center [39] at the national scale (longitude (73°40′–135°2.5′ E), latitude (3°52′–53°33′ N)). The second generation Deep Blue (DB) was expanded to cover brighter desert/urban areas and vegetated land surfaces, which preferably makes up for deficiencies in the Dark Target (DT) algorithms [40,41]. However, the spatial resolution of the Aqua Level 2 AOD using DB algorithms is 10 × 10 km, while the spatial resolution of the Aqua Level 2 AOD using DT algorithms reaches 3 × 3 km. Thus, the AOD datasets were fused by 3 km DT AOD and 10 km DB AOD, based on the concept of complementary advantages, in order to make merging AOD possess advantages on both spatial resolution and spatial coverage [42]. Moreover, only retrievals reaching the required quality assurance (QA) were used (corresponding to flag QA = 3 for DT; flag QA = 2 or QA = 3 for DB), ensuring the accuracy of the fused AOD.

2.3. Aerological and Surface Meteorological Parameters

Aerological parameters, including PBLH, and surface meteorological parameters, consisting of surface relative humidity, u-components, and v-components of surface winds, surface temperature, and surface atmospheric pressure, were collected from the National Centers for Environmental Prediction (NCEP) reanalysis datasets with 1° spatial resolution. Atmospheric product and land surface data taken every six hours are available in the NCEP datasets, which are available on its website [43].

2.4. Satellite-Derived EVI and NO$_2$ Data

The Enhanced Vegetation Index (EVI), which is calculated by surface reflectance in near-infrared, red, and blue bands, is an optimized vegetation index to represent vegetation biomass. The EVI, instead of the normalized difference vegetation index (NDVI) data, was adopted in this study to simply characterize the reduction effect by vegetation on PM$_{2.5}$ concentrations because the EVI is more sensitive to variations in regions having high biomass, which is an obvious advantage over NDVI [44]. Although the calculation of EVI is similar to NDVI, the distortions caused by atmospheric particles in the reflected light have been corrected, and the EVI product barely becomes saturated when scanning regions containing large amounts of chlorophyll [45]. EVI data with 1 km spatial resolution and 16-day temporal resolution was collected from the NASA LAADS website [39].

The daily tropospheric column density of NO$_2$ were collected from the NASA OMI level 2 nitrogen dioxide dataset with 0.25° spatial resolution [46]. The OMI NO$_2$ algorithm could compute accurate vertical column densities from NO$_2$ slant column densities, retrieved by spectral fitting. Since NO$_2$ is a short-life trace gas and has a tight relation to anthropogenic emissions and energy consumption [47–50], we utilized the satellite-derived NO$_2$ molar concentration as a simplified proxy of anthropogenic emissions.

2.5. Data Integration

From the perspective of time, the Aqua MODIS and Aura-OMI passes the equator at approximately 1:30 p.m. local time, thus all the aerological and surface meteorological variables were correspondingly selected around 2:00 p.m. local time (corresponding to UTC = 6:00 a.m.). Moreover, the daily NO$_2$ dataset and 16-day EVI dataset were respectively utilized to represent the daily extent of anthropogenic emissions and vegetation coverage for 16 days. In addition, a Kriging resampling approach was applied to ensure spatial consistency of all independent variables, which were demonstrated in Table 1 in detail. Moreover, the meteorological parameters and AOD values were both selected from the pixel in which the ground-level monitor is located.

Table 1. Relevant Level 2 SDS titles and contents for Aqua MODIS AOD at 550 nm.

Data	Source	Temporal Resolution	Spatial Resolution	Spatial Resolution after Resampling
PM$_{2.5}$	Ground-level Measurement	1 h	-	-
DT-AOD	Aqua-MODIS	1 day	3 km	3 km
DB-AOD	Aqua-MODIS	1 day	10 km	3 km
Meteorological Parameters	NCEP Reanalysis	6 h	100 km	3 km
NO$_2$	Aura-OMI	1 day	25 km	3 km
EVI	Aqua-MODIS	16 days	1 km	3 km

DT: Dark Target; DB: Deep Blue; EVI: Enhanced Vegetation Index; AOD: Aerosol Optical Depth; MODIS: Moderate Resolution Imaging Spectroradiometer; NCEP: National Centers for Environmental Prediction; OMI: Ozone Measuring Instrument; SDS: Safety data sheet.

2.6. Model Development, Comparison, and Validation

Because previous research has shown that the relationship between AOD and PM$_{2.5}$ obviously varies according to the spatial context, and the correlation coefficients could lead to poor accuracy of estimation when using global parameters [36]. To solve this problem, a GWR model has been established in this study, and the adaptive Gaussian bandwidth search method was utilized to accommodate the uneven distribution of ground-monitoring stations. The structure of the GWR model developed in this study is expressed in the following equation:

$$
\begin{aligned}
PM_{2.5,l,d} &= \beta_{0,l,d} + \beta_{1,l,d}Revised\_AOD_{l,d} + \beta_{2,l,d}ST_{l,d} + \beta_{3,l,d}RH_{l,d} + \beta_{4,l,d}PS_{l,d} \\
&\quad + \beta_{5,l,d}WS_{l,d} + \beta_{6,l,d}NO_{2,l,d} + \beta_{7,l,d}EVI_{l,d}
\end{aligned} \tag{1}
$$

where the $PM_{2.5,l,d}$ ($\mu g/m^3$) is the ground-level $PM_{2.5}$ concentration at location l on day d; $\beta_{0,l,d}$ denotes the intercept at location l on day d; $\beta_{0,l,d}$ to $\beta_{7,l,d}$ represent location-specific slopes; $Revised\_AOD_{l,d}$ (no unit) is the Aqua-MODIS AOD fused products revised by PBLH (m) at location l on day d. As demonstrated in previous studies, physics corrections based on vertical distribution could make remarkable improvement in the relationship between AOD and PM [29,51]. Because the ground monitoring stations measured mass concentration data of near ground $PM_{2.5}$, optical parameters for the ambient atmosphere should be measured instead of satellite-derived AOD that characterizes the entire atmospheric column. $ST_{l,d}$, $RH_{l,d}$, $PS_{l,d}$ and $WS_{l,d}$ are the surface temperature (K), surface relative humidity (%), atmospheric pressure (Pa), and surface wind speed (m/s), respectively, at location l on day d. $NO_{2,l,d}$ represents the column molar concentration of NO_2 at location l on day d, and $EVI_{l,d}$ represents the enhanced vegetation index at location l on 16-day d.

Moreover, to examine the effectiveness of introducing NO_2 and EVI into the GWR model as representatives of the anthropogenic emissions and the reduction effect by vegetation on $PM_{2.5}$. As a contrast, a GWR model without parameters of NO_2 and EVI was established using the same meteorological factors:

$$
PM_{2.5,l,d} = \beta_{0,l,d} + \beta_{1,l,d}Revised\_AOD_{l,d} + \beta_{2,l,d}ST_{l,d} + \beta_{3,l,d}RH_{l,d} + \beta_{4,l,d}PS_{l,d} + \beta_{5,l,d}WS_{l,d} \tag{2}
$$

In addition, a 10-fold cross validation analysis [52] was conducted to validate the quality of the model by comparing the estimated $PM_{2.5}$ against the monitoring values. The entire dataset was randomly split into 10 folds, with around ten percent of the total data in each subset, and the model was then fitted by nine folds with one fold set for validation in each cross-validation circle. This process was completely repeated 10 times so as to validate every fold. Furthermore, the estimation equation, decision coefficient R^2, and mean absolute error (MAE, $\mu g/m^3$) were calculated to evaluate the model performance.

3. Results and Discussion

3.1. Descriptive Statistics

The histograms and descriptive statistics of all the variables in the GWR model are illustrated in Figure 2, including the dependent variable and independent variables. It demonstrates that, apart from the surface air pressure displaying a bimodal distribution, which is possibly caused by the obvious elevation difference in southwest China, the remaining variables were approximately log-normal distributed. Overall, the mass concentrations of $PM_{2.5}$ ranged from 1 to 864.5 $\mu g/m^3$ with an annual average of 50.38 $\mu g/m^3$ and standard deviation (Std. Dev.) of 45.33 $\mu g/m^3$. The AOD frequency histograms have a shape similar to the measured $PM_{2.5}$ with an annual average AOD value of 497.49 and Std. Dev. of 470.72. Considering the Chinese standard of ambient air quality [53], the averaged mass concentration of $PM_{2.5}$ ranging from 2014 to 2015 exceeded the level 2 standard (35 $\mu g/m^3$).
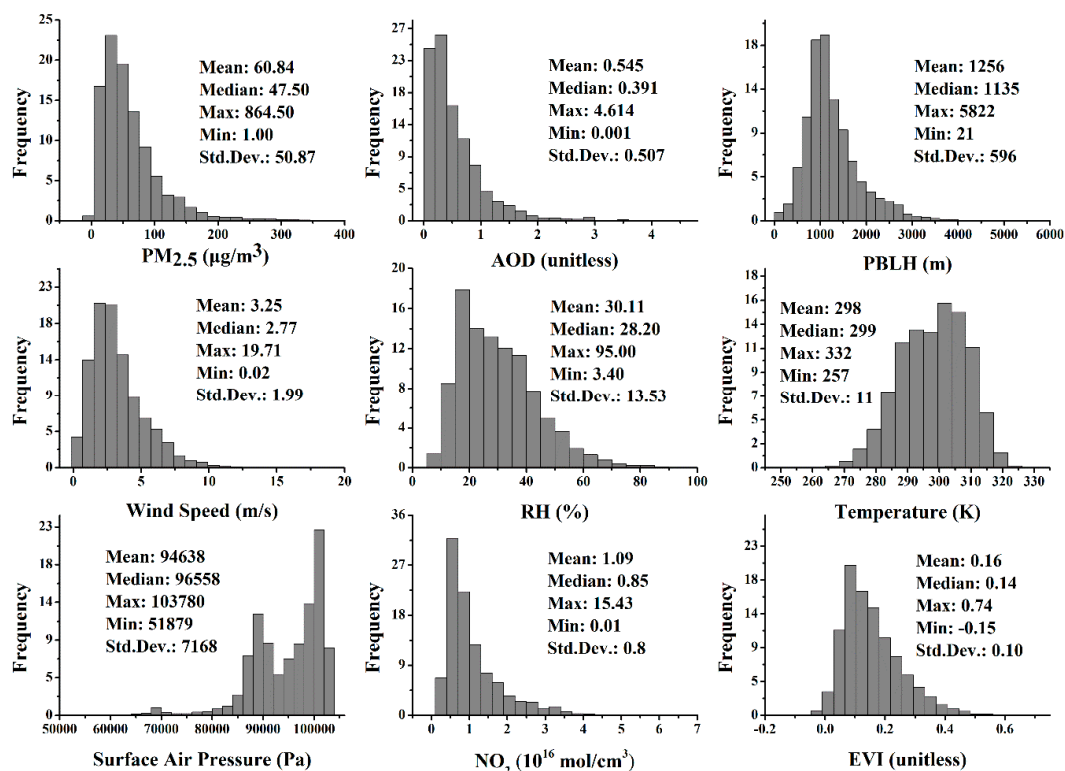
Figure 2. Histograms and descriptive statistics for $PM_{2.5}$, AOD, Planetary Boundary Layer Height (PBLH), wind speed, surface relative humidity (RH), surface temperature, surface air pressure, NO_2 column density, and EVI in the model fitting.

3.2. Model Fitting, Validation, and Comparison

The mass concentrations of $PM_{2.5}$ and corresponding estimations were obtained across China from 1 January 2014 to 31 December 2015. The original GWR model, the compared GWR model only adding NO_2, the compared GWR model only adding EVI, and newly developed GWR model were tested using the same datasets. There existed 119,885 pieces of data added to the model, and the cross-validation (CV) results for the GWR model are shown in Figure 3. The R^2 of the CV validation increased from 0.77 to 0.78 when only adding NO_2, with MAE decreased from 15.81 $\mu g/m^3$ to 15.08 $\mu g/m^3$. In addition, the R^2 of the CV validation increased from 0.77 to 0.82 when only adding EVI, with MAE decreased from 15.81 $\mu g/m^3$ to 13.83 $\mu g/m^3$. It showed that the introduction of NO_2 into the GWR model slightly improved the performance of model, while the introduction of EVI into the GWR model could substantially improve the performance of model. The R^2 of the CV validation increased from 0.77 to 0.87 when adding two parameters, which means that both parameters are relevant to the new developed GWR model. This two-year estimation result could account for approximately 87% of the variability in the corresponding $PM_{2.5}$ mass concentrations, which was relatively great at the national scale when comparing to other studies in China (cross validation R^2 achieved 0.64 and 0.79 in annual average, respectively) [38,54]. Moreover, the MAE calculated from the new model decrease from 15.81 $\mu g/m^3$ to 11.84 $\mu g/m^3$ against the original model, indicating that $PM_{2.5}$ estimated using the GWR model with NO_2 and EVI agreed better with the measurements. Moreover, according to the linear regression results, the regression line (solid black) of the new model better fit the actual line (dotted black), which illustrates that the introduction of NO_2 and EVI into GWR model could improve the estimation of $PM_{2.5}$, since it could achieve higher R^2 and better consistency with measurements.

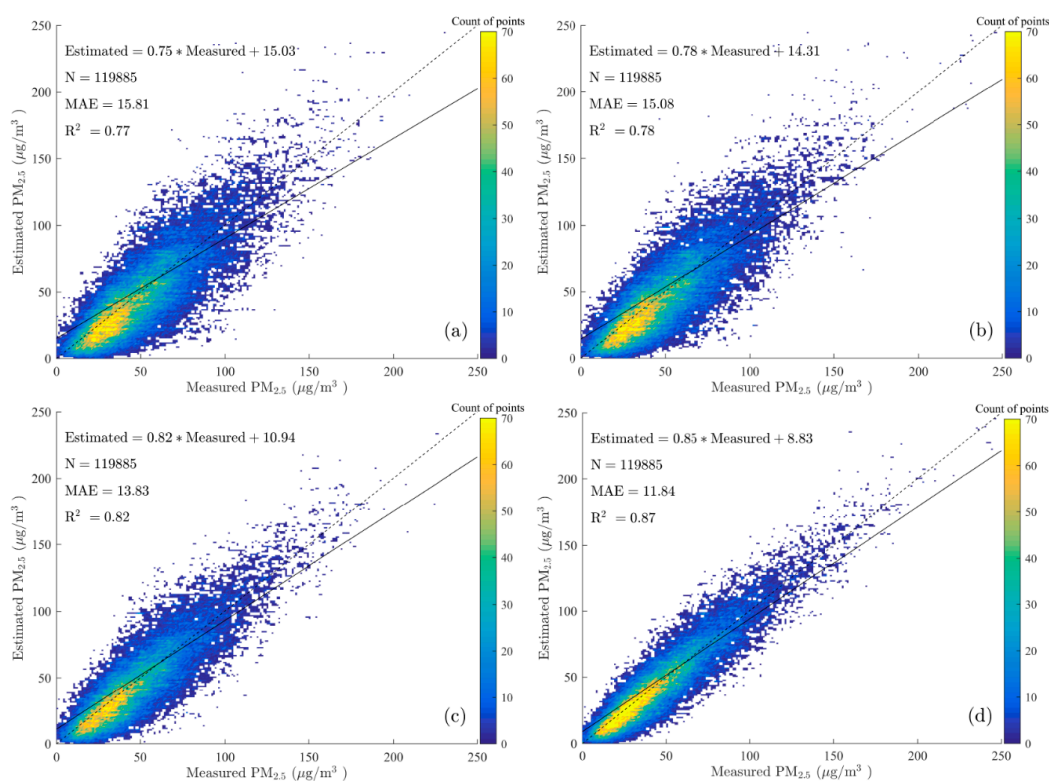*Int. J. Environ. Res. Public Health* **2016**, *13*, 1215

7 of 12

Figure 3. Scatter plot of model fitting and cross-validation for the GWR model: results of classical GWR model with vertical corrected AOD and meteorological parameters (**a**); results of GWR model only adding NO_2 (**b**); results of GWR model only adding EVI (**c**); and results of new GWR model adding NO_2 and EVI (**d**). The solid line and dotted line are the regression line, and y = x reference line, respectively.

However, the slope of the linear fitting equation was less than 1.0 and the intercept was positive, which suggests that the model is inclined to overestimate when the measurements of $PM_{2.5}$ are less than around 60 $\mu g/m^3$, and to underestimate when the measurements of $PM_{2.5}$ are larger than approximately 60 $\mu g/m^3$. Furthermore, the demarcation point, which was calculated by the point of intersection of linear fitting line and y = x reference line, was roughly equal in both GWR models. This phenomenon was probably caused by a mechanism of the GWR model that the coefficients of variables tend to be similar when they are geographically close to each other; therefore, the estimated values seem to be slightly averaged in a small region. Therefore, the particular value at an intersection point depends on the measured value of the dependent variable ($PM_{2.5}$) to a large extent.

3.3. Annual Estimation of $PM_{2.5}$ Mass Concentration

The estimated annual averaged $PM_{2.5}$ mass concentrations in 2014 and 2015 are illustrated in Figure 4. From a macro perspective, the spatial distributions of $PM_{2.5}$ are generally consistent from the year 2014 to 2015. The highest values of $PM_{2.5}$ were observed in the Jing-Jin-Ji Region (including Beijing, Tianjin, and Hebei), followed by Central China (including Hunan, Hubei, and Henan), and the Xinjiang Autonomous Region. In the Jing-Jin-Ji Region, the annual averaged $PM_{2.5}$ mass concentrations were generally higher than 80 $\mu g/m^3$ in 2014, and higher than 60 $\mu g/m^3$ in 2015. High levels of industrialization and urbanization, as well as the activities of dense human populations, have led to severe $PM_{2.5}$ pollution in these areas [55,56]. Based on the World Health Organization (WHO) Air Quality Interim Target (IT) levels, WHO IT-1 set the $PM_{2.5}$ mass concentration standard of 35 $\mu g/m^3$ [57], which means that most of regions in the North China Plain still suffer from severe fine particulate pollution. The situation is similar in central China, where most regions slightly exceeded

Int. J. Environ. Res. Public Health **2016**, *13*, 1215

8 of 12

the WHO IT-1 standard until 2015. The cleanest regions are in Tibet, Yunnan, and Hainan, where the annual average $PM_{2.5}$ values are generally lower than 20 µg/m³.
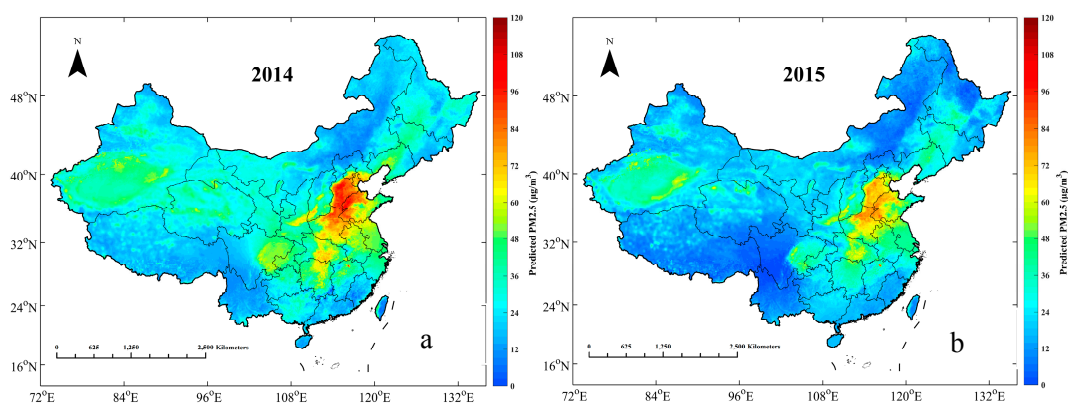

Figure 4. Estimations of annual averaged AOD-derived $PM_{2.5}$ in 2014 (**a**) and 2015 (**b**) when corresponding dataset values were available.

Nevertheless, the policy-driven efforts in energy conservation and emission reduction should not be ignored. Although there still exists $PM_{2.5}$ pollution in many residential areas, the apparent decrease in the overall trend is worth recognition. Not only the severity of $PM_{2.5}$ pollution but also the spatial coverage of heavy $PM_{2.5}$ pollution was alleviated, to a certain extent, from 2014 to 2015, especially in the North China Plain, Central Plain, scattered regions in the northeastern area and along the southern coast.

Although the model was demonstrated to estimate the spatial distribution of $PM_{2.5}$ effectively in most of areas in China, there still exist estimation errors in several regions. For instance, the mass concentrations of $PM_{2.5}$ in the Xinjiang Autonomous Region should be relatively high because the Tarim Basin, which is located in the southern section of the Xinjiang Autonomous Region, is mostly covered by the Taklimakan Desert, where dust aerosols come mostly from primal generation and entrained effects across eastern Asia [58]. However, the prediction results demonstrated that the annual averaged mass concentration of $PM_{2.5}$ in the Xinjiang Autonomous Region were less than 70 µg/m³, which was slightly below the measurements. The possible reason for this phenomenon in the model prediction is the introduction of NO_2. As widely acknowledged, the Xinjiang Autonomous Region is mostly covered by desert, which leads to relatively lower density of NO_2 measured by satellite. Thus, due to the positive fitted coefficients of NO_2, the prediction results would be less than measurements when there was no ground air-quality monitoring station in the desert. Moreover, the predictions of $PM_{2.5}$ in 2014 in Tibet, Qinghai, Gansu, northern Inner Mongolia, and western Sichuan were a little bit overestimated. This overestimation phenomenon primarily resulted from uneven distribution of the ground level $PM_{2.5}$ monitoring sites in 2014. There was primary coverage in large urban centers and sparse coverage in rural areas, especially in the western regions of the country. Less coverage of ground level $PM_{2.5}$ monitoring stations in these regions would directly result in the increase of bandwidth in the GWR model, further leading to the consequence that regional modeling would be influenced primarily by the farther surrounding areas. Since the GWR model adopts an adaptive bandwidth searching method, the bandwidth will increase when the ground stations are sparse, further decreasing the effects of model performance. However, along with construction of the Chinese air-quality monitoring network, the situation was alleviated in 2015, and this issue will gradually be resolved. In the current data conditions, the model could only achieve anticipative efficacy of estimation in eastern China.

4. Conclusions

The estimation of mass concentrations of $PM_{2.5}$ at the national scale was conducted using a GWR model, by introducing NO_2 and EVI, combined with fused Aqua MODIS AOD and meteorological parameters. According to the results of 10-fold cross-validation, the introduction of NO_2 and EVI as independent variables in the GWR model obviously improved the quality of estimation, where the decision coefficient R^2 increased from 0.77 to 0.87, and MAE decreased from 15.81 to 11.84 $\mu g/m^3$ against the results from the original model. Moreover, the newly developed model and original model both tended to overestimate when the measured value of $PM_{2.5}$ was less than around 60 $\mu g/m^3$, but tended to underestimate when the measured value was larger than approximately 60 $\mu g/m^3$. In addition, this particular value that marks this boundary, which was calculated from the intersection point of the linear fitting line and y = x as the reference line, depends on the measurements of dependent variable ($PM_{2.5}$) to a large extent.

According to the spatial distribution of annual average $PM_{2.5}$ mass concentrations in 2014 and 2015, the highest values of $PM_{2.5}$ arose in the Jing-Jin-Ji Region, followed by Central China and the Xinjiang Autonomous Region. Furthermore, the NO_2 embedded GWR model would be inclined to underestimate in the desert regions that possess relatively low density of NO_2 measured by satellite. In addition, regional modeling would be influenced more by surrounding areas when the coverage of ground level monitoring stations is insufficient. Thus, in current data conditions, it is hard to achieve anticipative performance of estimation in western China. Nevertheless, this situation was alleviated in 2015 and will gradually be resolved following construction of the air-quality monitoring network in China.

In general, the introduction of NO_2 and EVI into the GWR model could more effectively estimate $PM_{2.5}$ at the national scale compared to the original GWR model using satellite-derived AOD and meteorological parameters. Further research will be conducted on the modeling algorithm and source apportionment of $PM_{2.5}$ to achieve better performance. The estimation of $PM_{2.5}$ mass concentrations at the national scale could provide a reasonable reference for assessing health impacts in China, and for examining the effectiveness of the emission control strategies under implementation.

Author Contributions: The research topic was designed by Tianhao Zhang. Tianhao Zhang and Yuxi Ji conducted the experiment, and the paper was written by Wei Gong and Wei Wang. Tianhao Zhang, Zhongmin Zhu, and Yusi Huang checked the experimental data and examined the experimental results. All authors agreed to submission of the manuscript.

Conflicts of Interest: The authors declare no conflict of interest.

References

1. Kaufman, Y.J.; Tanré, D.; Boucher, O. A satellite view of aerosols in the climate system. *Nature* **2002**, *419*, 215–223. [CrossRef] [PubMed]
2. Peters, A.; Dockery, D.W.; Muller, J.E.; Mittleman, M.A. Increased particulate air pollution and the triggering of myocardial infarction. *Circulation* **2001**, *103*, 2810–2815. [CrossRef] [PubMed]
3. See, S.W.; Balasubramanian, R. Chemical characteristics of fine particles emitted from different gas cooking methods. *Atmos. Environ.* **2008**, *42*, 8852–8862. [CrossRef]
4. Van Donkelaar, A.; Martin, R.V.; Brauer, M.; Kahn, R.; Levy, R.; Verduzco, C.; Villeneuve, P.J. *Global Estimates of Ambient Fine Particulate Matter Concentrations from Satellite-Based Aerosol Optical Depth: Development and Application*; University of British Columbia: Vancouver, BC, Canada, 2015.
5. Brunekreef, B.; Forsberg, B. Epidemiological evidence of effects of coarse airborne particles on health. *Eur. Respir. J.* **2005**, *26*, 309–318. [CrossRef] [PubMed]

Int. J. Environ. Res. Public Health **2016**, *13*, 1215

10 of 12

6. Künzli, N.; Jerrett, M.; Mack, W.J.; Beckerman, B.; LaBree, L.; Gilliland, F.; Thomas, D.; Peters, J.; Hodis, H.N. Ambient air pollution and atherosclerosis in Los Angeles. *Environ. Health Perspect.* **2005**, *113*, 201–206. [CrossRef] [PubMed]

7. Zhang, Q.; He, K.; Huo, H. Policy: Cleaning China's air. *Nature* **2012**, *484*, 161–162. [PubMed]

8. Chan, C.K.; Yao, X. Air pollution in mega cities in China. *Atmos. Environ.* **2008**, *42*, 1–42. [CrossRef]

9. Hu, X.; Waller, L.A.; Al-Hamdan, M.Z.; Crosson, W.L.; Estes, M.G.; Estes, S.M.; Quattrochi, D.A.; Sarnat, J.A.; Liu, Y. Estimating ground-level $PM_{2.5}$ concentrations in the southeastern U.S. using geographically weighted regression. *Environ. Res.* **2013**, *121*, 1–10. [CrossRef] [PubMed]

10. Hu, X.; Waller, L.A.; Lyapustin, A.; Wang, Y.; Al-Hamdan, M.Z.; Crosson, W.L.; Estes, M.G.; Estes, S.M.; Quattrochi, D.A.; Puttaswamy, S.J. Estimating ground-level $PM_{2.5}$ concentrations in the southeastern United States using MAIAC AOD retrievals and a two-stage model. *Remote Sens. Environ.* **2014**, *140*, 220–232. [CrossRef]

11. Van Donkelaar, A.; Martin, R.V.; Brauer, M.; Kahn, R.; Levy, R.; Verduzco, C.; Villeneuve, P.J. Global estimates of ambient fine particulate matter concentrations from satellite-based aerosol optical depth: Development and application. *Environ. Health Perspect.* **2010**, *118*, 847. [CrossRef] [PubMed]

12. Che, H.; Xia, X.; Zhu, J.; Wang, H.; Wang, Y.; Sun, J.; Zhang, X.; Shi, G. Aerosol optical properties under the condition of heavy haze over an urban site of Beijing, China. *Environ. Sci. Pollut. Res.* **2015**, *22*, 1043–1053. [CrossRef] [PubMed]

13. Chu, D.A.; Kaufman, Y.; Zibordi, G.; Chern, J.; Mao, J.; Li, C.; Holben, B. Global monitoring of air pollution over land from the Earth Observing System-Terra Moderate Resolution Imaging Spectroradiometer (MODIS). *J. Geophys. Res. Atmos.* **2003**, *108*. [CrossRef]

14. Koelemeijer, R.; Homan, C.; Matthijsen, J. Comparison of spatial and temporal variations of aerosol optical thickness and particulate matter over Europe. *Atmos. Environ.* **2006**, *40*, 5304–5315. [CrossRef]

15. Gupta, P.; Christopher, S.A.; Wang, J.; Gehrig, R.; Lee, Y.; Kumar, N. Satellite remote sensing of particulate matter and air quality assessment over global cities. *Atmos. Environ.* **2006**, *40*, 5880–5892. [CrossRef]

16. Che, H.; Xia, X.; Zhu, J.; Li, Z.; Dubovik, O.; Holben, B.; Goloub, P.; Chen, H.; Estelles, V.; Cuevas-Agulló, E. Column aerosol optical properties and aerosol radiative forcing during a serious haze-fog month over North China Plain in 2013 based on ground-based sunphotometer measurements. *Atmos. Chem. Phys.* **2014**, *14*, 2125–2138. [CrossRef]

17. Gupta, P.; Christopher, S.A. Particulate matter air quality assessment using integrated surface, satellite, and meteorological products: Multiple regression approach. *J. Geophys. Res. Atmos.* **2009**, *114*. [CrossRef]

18. Liu, Y.; Sarnat, J.A.; Kilaru, V.; Jacob, D.J.; Koutrakis, P. Estimating ground-level $PM_{2.5}$ in the eastern United States using satellite remote sensing. *Environ. Sci. Technol.* **2005**, *39*, 3269–3278. [CrossRef] [PubMed]

19. Wallace, J.; Kanaroglou, P. An investigation of air pollution in southern Ontario, Canada, with MODIS and MISR aerosol data. In Proceedings of the Geoscience and Remote Sensing Symposium, Barcelona, Spain, 23–28 July 2007; pp. 4311–4314.

20. Lee, H.; Liu, Y.; Coull, B.; Schwartz, J.; Koutrakis, P. A novel calibration approach of MODIS AOD data to predict $PM_{2.5}$ concentrations. *Atmos. Chem. Phys. Discuss.* **2011**, *11*, 9769–9795. [CrossRef]

21. Yap, X.; Hashim, M. A robust calibration approach for PM_{10} prediction from MODIS aerosol optical depth. *Atmos. Chem. Phys. Discuss.* **2012**, *12*, 31483–31505. [CrossRef]

22. Wu, Y.; Guo, J.; Zhang, X.; Tian, X.; Zhang, J.; Wang, Y.; Duan, J.; Li, X. Synergy of satellite and ground based observations in estimation of particulate matter in eastern China. *Sci. Total Environ.* **2012**, *433*, 20–30. [CrossRef] [PubMed]

23. Geng, G.; Zhang, Q.; Martin, R.V.; van Donkelaar, A.; Huo, H.; Che, H.; Lin, J.; He, K. Estimating long-term $PM_{2.5}$ concentrations in China using satellite-based aerosol optical depth and a chemical transport model. *Remote Sens. Environ.* **2015**, *166*, 262–270. [CrossRef]

24. Zhang, Y.; Li, Z. Remote sensing of atmospheric fine particulate matter ($PM_{2.5}$) mass concentration near the ground from satellite observation. *Remote Sens. Environ.* **2015**, *160*, 252–262. [CrossRef]

25. Li, Z.; Zhang, Y.; Shao, J.; Li, B.; Hong, J.; Liu, D.; Li, D.; Wei, P.; Li, W.; Li, L. Remote sensing of atmospheric particulate mass of dry $PM_{2.5}$ near the ground: Method validation using ground-based measurements. *Remote Sens. Environ.* **2016**, *173*, 59–68. [CrossRef]

26. Stewart Fotheringham, A.; Charlton, M.; Brunsdon, C. The geography of parameter space: An investigation of spatial non-stationarity. *Int. J. Geogr. Inform. Syst.* **1996**, *10*, 605–627. [CrossRef]

Int. J. Environ. Res. Public Health **2016**, *13*, 1215

11 of 12

27. Zhao, N.; Yang, Y.; Zhou, X. Application of geographically weighted regression in estimating the effect of climate and site conditions on vegetation distribution in Haihe catchment, China. *Plant Ecol.* **2010**, *209*, 349–359. [CrossRef]

28. Wang, Z.; Chen, L.; Tao, J.; Zhang, Y.; Su, L. Satellite-based estimation of regional particulate matter (PM) in Beijing using vertical-and-RH correcting method. *Remote Sens. Environ.* **2010**, *114*, 50–63. [CrossRef]

29. Zhang, T.; Gong, W.; Zhu, Z.; Sun, K.; Huang, Y.; Ji, Y. Semi-physical estimates of national-scale PM_{10} concentrations in China using a satellite-based geographically weighted regression model. *Atmosphere* **2016**, *7*, 88. [CrossRef]

30. Kloog, I.; Melly, S.J.; Ridgway, W.L.; Coull, B.A.; Schwartz, J. Using new satellite based exposure methods to study the association between pregnancy $PM_{2.5}$ exposure, premature birth and birth weight in massachusetts. *Environ. Health* **2012**, *11*, 40. [CrossRef] [PubMed]

31. China Environmental Monitoring Center. Available online: http://113.108.142.147:20035/emcpublish/ (accessed on 6 December 2016).

32. Determination of Atmospheric Articles PM_{10} and $PM_{2.5}$ in Ambient Air by Gravimetric Method. Available online: http://english.mep.gov.cn/standards_reports/standards/Air_Environment/air_method/201111/t20111101_219390.htm (accessed on 6 December 2016).

33. Remer, L.A.; Kaufman, Y.; Tanré, D.; Mattoo, S.; Chu, D.; Martins, J.V.; Li, R.-R.; Ichoku, C.; Levy, R.; Kleidman, R. The MODIS aerosol algorithm, products, and validation. *J. Atmos. Sci.* **2005**, *62*, 947–973. [CrossRef]

34. Levy, R.C.; Remer, L.A.; Mattoo, S.; Vermote, E.F.; Kaufman, Y.J. Second-generation operational algorithm: Retrieval of aerosol properties over land from inversion of moderate resolution imaging spectroradiometer spectral reflectance. *J. Geophys. Res. Atmos.* **2007**, *112*. [CrossRef]

35. Chu, D.; Kaufman, Y.; Ichoku, C.; Remer, L.; Tanré, D.; Holben, B. Validation of MODIS aerosol optical depth retrieval over land. *Geophys. Res. Lett.* **2002**, *29*. [CrossRef]

36. Engel-Cox, J.A.; Holloman, C.H.; Coutant, B.W.; Hoff, R.M. Qualitative and quantitative evaluation of MODIS satellite sensor data for regional and urban scale air quality. *Atmos. Environ.* **2004**, *38*, 2495–2509. [CrossRef]

37. Ma, Z.; Hu, X.; Sayer, A.M.; Levy, R.; Zhang, Q.; Xue, Y.; Tong, S.; Bi, J.; Huang, L.; Liu, Y. Satellite-based spatiotemporal trends in $PM_{2.5}$ concentrations: China, 2004–2013. *Environ. Health Perspect.* **2015**, *124*. [CrossRef] [PubMed]

38. You, W.; Zang, Z.; Zhang, L.; Li, Y.; Pan, X.; Wang, W. National-scale estimates of ground-level $PM_{2.5}$ concentration in China using geographically weighted regression based on 3 km resolution MODIS AOD. *Remote Sens.* **2016**, *8*, 184. [CrossRef]

39. NASA LAADS MODIS. Available online: http://ladsweb.nascom.nasa.gov/ (accessed on 6 December 2016).

40. Sayer, A.; Hsu, N.; Bettenhausen, C.; Jeong, M.J. Validation and uncertainty estimates for MODIS Collection 6 "Deep Blue" aerosol data. *J. Geophys. Res. Atmos.* **2013**, *118*, 7864–7872. [CrossRef]

41. Sayer, A.; Munchak, L.; Hsu, N.; Levy, R.; Bettenhausen, C.; Jeong, M.J. Modis collection 6 aerosol products: Comparison between aqua's E-deep blue, dark target, and "merged" data sets, and usage recommendations. *J. Geophys. Res. Atmos.* **2014**, *119*, 13965–13989. [CrossRef]

42. Zhang, T.; Liu, G.; Zhu, Z.; Gong, W.; Ji, Y.; Huang, Y. Real-time estimation of satellite-derived $PM_{2.5}$ based on a semi-physical geographically weighted regression model. *Int. J. Environ. Res. Public Health* **2016**, *13*, 974. [CrossRef] [PubMed]

43. CFS NCEP Reanalysis Meteorological Datasource. Available online: http://cfs.ncep.noaa.gov/ (accessed on 6 December 2016).

44. Wang, Z.; Liu, C.; Huete, A. From AVHRR-NDVI to MODIS-EVI: Advances in vegetation index research. *Acta Ecol. Sin.* **2002**, *23*, 979–987.

45. Weier, J.; Herring, D. Measuring Vegetation (NDVI and EVI). Available online: http://earthobservatory.nasa.gov/Features/MeasuringVegetation/ (accessed on 6 December 2016).

46. NASA Aura OMI. Available online: http://disc.sci.gsfc.nasa.gov/Aura/data-holdings/OMI/omno2_v003.shtml (accessed on 6 December 2016).

47. Zhang, Q.; Geng, G.; Wang, S.; Richter, A.; He, K. Satellite remote sensing of changes in no X emissions over China during 1996–2010. *Chin. Sci. Bull.* **2012**, *57*, 2857–2864. [CrossRef]

Int. J. Environ. Res. Public Health **2016**, *13*, 1215

12 of 12

48. Zheng, Y.; Zhang, Q.; Liu, Y.; Geng, G.; He, K. Estimating ground-level PM$_{2.5}$ concentrations over three megalopolises in China using satellite-derived aerosol optical depth measurements. *Atmos. Environ.* **2016**, *124*, 232–242. [CrossRef]

49. Zhang, T.; Zhu, Z.; Gong, W.; Xiang, H.; Fang, R. Characteristics of fine particles in an urban atmosphere—Relationships with meteorological parameters and trace gases. *Int. J. Environ. Res. Public Health* **2016**, *13*, 807. [CrossRef] [PubMed]

50. Zhang, T.; Zhu, Z.; Gong, W.; Xiang, H.; Li, Y.; Cui, Z. Characteristics of ultrafine particles and their relationships with meteorological factors and trace gases in Wuhan, central China. *Atmosphere* **2016**, *7*, 96. [CrossRef]

51. Song, W.; Jia, H.; Huang, J.; Zhang, Y. A satellite-based geographically weighted regression model for regional PM$_{2.5}$ estimation over the pearl river delta region in China. *Remote Sens. Environ.* **2014**, *154*, 1–7. [CrossRef]

52. Rodriguez, J.D.; Perez, A.; Lozano, J.A. Sensitivity analysis of K-fold cross validation in prediction error estimation. *IEEE Trans. Pattern Anal. Mach. Intell.* **2010**, *32*, 569–575. [CrossRef] [PubMed]

53. China, M. *Ambient Air Quality Standards. GB 3095-2012*; China Environmental Science Press: Beijing, China, 2012.

54. Ma, Z.; Hu, X.; Huang, L.; Bi, J.; Liu, Y. Estimating ground-level PM$_{2.5}$ in China using satellite remote sensing. *Environ. Sci. Technol.* **2014**, *48*, 7436–7444. [CrossRef] [PubMed]

55. Quan, J.; Zhang, Q.; He, H.; Liu, J.; Huang, M.; Jin, H. Analysis of the formation of fog and haze in North China Plain (NCP). *Atmos. Chem. Phys.* **2011**, *11*, 8205–8214. [CrossRef]

56. Tao, M.; Chen, L.; Su, L.; Tao, J. Satellite observation of regional haze pollution over the North China Plain. *J. Geophys. Res. Atmos.* **2012**, *117*. [CrossRef]

57. World Health Organization. *Air Quality Guidelines: Global Update 2005: Particulate Matter, Ozone, Nitrogen Dioxide, and Sulfur Dioxide*; World Health Organization: Geneva, Switzerland, 2006.

58. Huang, J.; Minnis, P.; Chen, B.; Huang, Z.; Liu, Z.; Zhao, Q.; Yi, Y.; Ayers, J.K. Long-range transport and vertical structure of Asian dust from Calipso and surface measurements during PACDEX. *J. Geophys. Res. Atmos.* **2008**, *113*. [CrossRef]